



CO oxidation over gold catalysts supported on CuO/Cu₂O both in O₂-rich and H₂-rich streams: Necessity of copper oxide

Caixia Qi*, Yuhua Zheng, Hui Lin, Huijuan Su, Xun Sun, Libo Sun

Shandong Applied Research Center of Gold Nanotechnology (Au-SDARC), School of Chemistry and Chemical Engineering, Yantai University, Yantai 264005, PR China



ARTICLE INFO

Keywords:
CO oxidation
Oxygen-rich stream
Hydrogen-rich stream
Au catalysts
Copper and cuprous oxides

ABSTRACT

In order to clarify the nature of cooperation effect of gold–copper in CO oxidation without disturb of substrate materials, in this work we prepared nano-sized copper and cuprous oxide with different morphologies followed by the deposition of gold nanoparticles. The reaction of CO oxidation under both hydrogen-rich and oxygen-rich streams was investigated over as-prepared CuO/Cu₂O materials and the corresponding supported gold catalysts. The characterizations reveal that in the un-reduced Au/Cu₂O samples, Au⁺–Cu²⁺ assemblies are dominant on the surface of Cu₂O substrate due to the spontaneous oxidation–reduction reaction of Au³⁺ and Cu⁺, while both of Au³⁺–Cu²⁺ and Au⁺–Cu²⁺ entireties are existed in the un-reduced Au/CuO sample and the former is dominant. A comprehensive analysis of the catalytic results over these samples for CO oxidation in both oxygen-rich and hydrogen-rich streams demonstrates that the CuO species (not Cu₂O) play a more critical role for the oxidation of CO and the improved catalytic activity of the Au/CuO catalyst can be attributed to the strong interactions of CuO support with nanogold particles.

1. Introduction

The CO preferential oxidation process (CO-PROX) has been widely recognized as one of the most promising and cost effective ways in providing pure hydrogen for the proton exchange membrane fuel cell. The key issues for the application of the CO-PROX process is to develop a highly active and selective catalyst for CO oxidation that performs well in a relatively wide temperature window (e.g. 60–120 °C) and has good resistance to both CO₂ and moisture [1]. In general, Pt (Ru)- Au, and Cu-based catalysts are three of main studied catalyst systems applied to CO-PROX reaction in recent researches with nice performance in different temperature range [2–4]. The sequence of their reaction temperatures with the similar conversion rate is in the order of Au catalyst < Cu catalyst < Pt(Ru) catalyst.

Supported gold catalysts are famous on their high activity at temperatures even lower than room temperature compared with the Cu and Pt catalysts. In addition, they are also known as free of CO₂ and their catalytic activities can even be promoted (not hindered as in Cu and Pt) by moisture [5,6]. However, the pure Au based catalysts also suffer from the relatively low selectivity for the CO oxidation under PROX conditions. On contrast, higher selectivity to CO₂ at moderate temperature is the advantage of Cu-based catalysts, which are unfortunately easy deactivated in the stream with higher amount of CO₂.

and moisture [7–9]. The combination of Au-Cu catalysts has shown much better results than single Au- and CuO-based catalyst in the process of CO-PROX reaction [10–13]. The Au-Cu cooperation effect was also demonstrated in numbers of reactions, like water gas shift [14] and aerobic oxidation of benzyl alcohol [15].

Our previous study [16] and the other work [17–19] explored that Au/CuOx species rather than AuCu nanoalloy play a main role in CO oxidation in CO-PROX process. However, it is still in intense debate on the details of active Au-Cu-O sites in the CO-PROX catalysts. Our previous results implied the importance of maintaining CuO in final catalyst for the CO-PROX reaction [16]. However, the presence of copper species with lower binding energy than Cu(II) and considerable amount of positively charged Au^{δ+} in the sample were confirmed by our XPS and H₂-TPR analysis. This strongly supposes a strong interaction between metallic Au nanoparticles with CuO that may lead to a transfer from Au⁰ to Cu²⁺ to form Cu(I) species. Cationic gold was claimed by several reports [20–22] responsible for the enhancement of the catalytic activity due to carbon monoxide activated by its vacant d-orbital. Negatively charged gold was also proposed [23–25] to be the active species due to its enhanced back-donation from Au d-electrons into the antibonding π* orbital of adsorbed carbon monoxide. In addition, the work done by Jia's group indicated that metallic gold was more active than ionic gold for CO oxidation [26].

* Corresponding author.

E-mail address: qjcx@ytu.edu.cn (C. Qi).

Copper has various oxidation states, such as Cu₂O and CuO. It was reported that Cu₂O was found to be more active than CuO for CO oxidation [27]. Few studies on the copper–ceria catalyst, a very promising candidate for the CO-PROX too, have demonstrated that active sites are related to interfacial Cu(I) species generated through a reductive process upon interaction with CO [28–30].

Most of works on AuCu bimetallic catalysts and Au/CuOx catalysts were deposited on a substrate of oxide/composites oxides [12,16–19] or other materials like metallic Cu support [31]. CuOx act as additives in these cases. The substrate surely make important contribution in stabilizing nanogold particles or providing oxygen vacancies or donate/or attract electrons to/from gold via metal–support interaction and therefore influencing the catalytic performance because the reaction of CO mainly takes place on the perimeter interface [32]. The influences in direction of electron transfer between gold and substrate/CuOx, and adsorbing sites of CO as well as further in catalytic activity may varies from different substrates, like the reducible substrate and non-reducible substrate.

In order to clarify the nature of Au-CuOx cooperation effects in CO oxidation without disturb of substrate materials, in this work we prepare nanometer copper oxide and cuprous oxide with different morphologies followed by the deposition of gold nanoparticles. Not only the PROX reaction, i.e., the oxidation of CO in hydrogen-rich stream but also the reaction of CO oxidation in oxygen-rich stream were investigated over as-prepared CuO/Cu₂O materials and the corresponding supported gold catalysts without reduction for better understanding the interaction between copper species and gold species in the process of CO oxidation via correlating the changes in electric structure of the studied samples and their catalytic performance in two kinds of reactive environment.

2. Experimental

2.1. The preparation of CuOx materials

The chemical precipitation method was used to synthesize Cu₂O with different morphologies [33–35]. CuCl₂·2H₂O, NaOH and ascorbic acid were used as the copper precursor, precipitant and reducing agent, respectively. By adjusting the mole ratio between surfactant PVP and CuCl₂, nano cuprous oxide with two different morphologies was prepared. The specific preparation process is as follows. Quantitative CuCl₂·2H₂O was dissolved in deionized water to prepare 0.01 M CuCl₂ solution. A certain amount of PVP was then dissolved in the CuCl₂ solution at 55 °C in water bath. After dropwise addition of 2 M NaOH solution, the reaction mixture was stirred magnetically for 0.5 h. 0.6 M ascorbic acid was added dropwise into the mixture and the mixture was stirred for another 3.0 h. The products were centrifuged and washed by deionized water and ethanol, respectively. The obtained solid products were dried at 60 °C in a vacuum oven for 6 h. When the mole ratio between surfactant PVP and CuCl₂ was 0, which means that there is no PVP added into the reaction system, the obtained Cu₂O was labeled as Cu₂O (I), while when mole ratio of PVP/CuCl₂ was kept at 30, the obtained Cu₂O was labeled as Cu₂O (II).

Copper oxide was prepared by the same procedure with that of Cu₂O except that ascorbic acid was not added.

2.2. The preparation of Au/CuOx catalysts by a modified deposition–precipitation method

A modified deposition–precipitation method developed by our group [7,36–38] was applied to prepare CuOx supported Au catalysts with a theoretical Au loading of 2.0 wt%. A certain amount of copper oxides was added into a solution of HAuCl₄·xH₂O with a pH of 9.0 that was adjusted by 1.0 M KOH solution and then was soaked into aqueous ammonia (pH = 9–10) for 24 h. The products were washed several times until no white precipitation was produced when using AgNO₃

solution tested. After drying in a vacuum oven overnight at 60 °C, the final Au/CuOx catalysts were obtained.

2.3. Characterizations

The atomic emission spectrometry was carried out by IRIS XSP inductive coupling plasma emission spectrograph (Thermo Electron Company, USA) to measure the actual contents of Au in the catalysts.

A XRD-6100 X-ray diffractometer (Shimadzu Corporation, Japan) was applied to identify the as-synthesized CuOx materials by using Cu K α (0.154 nm) radiation and graphite monochromator (40 kV, 30 mA) with a step size of 6°/min in the range of 10–80°.

An S-4800 scanning electron microscopy (Hitachi, Japan) with an accelerating voltage of 200 kV was performed to clarify the morphology of oxides of copper. A JEOL JEM-200 (JEOL Company, Tokyo, Japan) transmission electron microscopy (TEM) was applied at 200 kV accelerating voltage to evaluate the size distribution of gold particles for fresh gold catalysts. The samples were dispersed in ethanol and dropped on a carbon coated copper mesh and were dried at room temperature before SEM and TEM characterizations.

An autoChem II 2920 chemisorption analyzer (Micromeritic, USA) was performed for CO pulse chemisorption measurements. Before chemisorption, 200 mg of samples was pretreated at 100 °C for 60 min in a flow of 10 vol.% H₂ in argon and then cooled in helium flow down to the temperature of –116 °C. The standard operating conditions are as follow: CO content in pulses (10 vol.%), helium flowrate (30 ml/min), and pulse size (0.5 ml).

A TP-5080 temperature programmed desorption instrument (Tianjin Xianquan Co. Ltd., China) was adopted to investigate the reducibility of catalysts. 10 vol.% H₂ in argon was used as the carrier gas with a flowrate of 20 ml/min. The testing temperature was in the range of 20–450 °C with a heating rate of 10 °C/min.

An ESCALAB X-ray photoelectron spectroscopy instrument (Thermo Fisher Scientific Inc., USA) was employed to check the chemical states of copper and gold in the catalysts by using Mg-K α (E_b = 1253.6 eV) radiation with an accelerating voltage of 15 kV. The percentages of surface atoms of the elements in the catalysts were calculated by the areas of the binding energy after the correction and normalization. The organic polluted carbon (C1s: E = 284.6 eV) was used as the corrective standard of energy.

2.4. The catalytic testing of oxides of copper and their Au catalysts

The hydrogen-rich reformed gas mixture mainly includes H₂, CO₂, CO, and H₂O, which spontaneously generates complex chemical reactions in Table 1. A competition is therefore for the oxidation of CO and H₂ which have approximate thermodynamic values. The CO preferential oxidation process means that a little oxygen or air is added to the hydrogen rich gas. In the study, the feed gas mixture with the composition of 1.2 vol.% CO, 0.8 vol.% O₂, 50 vol.% H₂, and 48 vol.% N₂ was applied and the reaction was directly carried out over 200 mg of the unduced catalysts at the atmospheric pressure in a continuous flow fixed bed glass reactor with a flow rate of 50 ml/min. The products were analyzed on-line by using a GC-920 gas chromatography (Haixin Company, Shanghai, China) with a TCD detector and a molecular sieve 5A column capable of separating O₂, N₂, CH₄, and CO.

Table 1
the main reactions occurred in CO-PROX process.

Reaction equations	$\Delta H_{298\text{ K}}$ (kJ/mol)	$\Delta_f G_{298\text{ K}}$ (kJ/mol)
CO + 0.5O ₂ = CO ₂	–282.98	–257.19
H ₂ + 0.5O ₂ = H ₂ O	–241.82	–228.57
CO + H ₂ O = CO ₂ + H ₂	–41.16	–28.62
CO + 3H ₂ = CH ₄ + H ₂ O(g)	–206.10	–142.12
CO ₂ + 4H ₂ = CH ₄ + 2H ₂ O(g)	–164.91	–133.5

The reaction temperature was raised by the programmed technology with a heating rate of 2 °C/min in the range of 20–250 °C from a preset temperature to another. The products were analyzed twice in 30 min for reaching a steady state after the feed was sampled at each preset temperature. No methane was detected in this study.

The catalytic performances were defined in terms of conversion of CO (X_{CO}) and selectivity to CO_2 (S_{CO_2}), which were calculated according to the following equations:

$$X_{CO} (\%) = \frac{([CO]_{in} - [CO]_{out})}{[CO]_{in}} \times 100$$

$$X_{O_2} (\%) = \frac{([O_2]_{in} - [O_2]_{out})}{[O_2]_{in}} \times 100$$

$$S_{CO_2} (\%) = \frac{([CO]_{in} - [CO]_{out})}{2([O_2]_{in} - [O_2]_{out})} \times 100 = \frac{X_{CO}}{2X_{O_2}} \times 100$$

where $[CO]_{in}$ or $[O_2]_{in}$ is intake concentration, $[CO]_{out}$ or $[O_2]_{out}$ is output concentration.

The CO oxidation in oxygen-rich stream was carried out in a similar manner with the feed composition of 1.0 vol.% CO, 21 vol.% O₂, and 78 vol.% N₂.

3. Results

3.1. Identification of the as-synthesized oxides of copper

Fig. 1(a and b) shows the SEM images of Cu₂O (I) and Cu₂O (II). From the image, we can know that the Cu₂O shows regular cubic and cubooctahedral morphologies. The Cu₂O particles are uniform in size with good dispersion. When PVP was not used ($R = 0$), the Cu₂O particles showed cubic morphology with six square {1 1 0} planes in each unit cell. The length of Cu₂O particles was around 1.00 μm. When the mole ratio between surfactant PVP and CuCl₂ was kept at 30 ($R = 30$), the Cu₂O particles showed cubic-octahedral morphology with eight square {1 1 0} planes and six triangular {1 1 1} planes in each unit cell. The length of Cu₂O particles was around 1.00 μm with small particles.

Fig. 1c shows the SEM images of CuO with or without the use of PVP in preparation process. From the image, we can find that regular sheet CuO were obtained with uniform size regardless of usage of PVP. The particle size was around 300 nm in length, 150 nm in width and 5 nm in thickness.

In order to identify the purity and crystallinity of the as-synthesized copper oxides, the X-ray diffractions (XRD) were performed and the corresponding results for Cu₂O and CuO are given in **Fig. 2(a and b)**, respectively. It can be seen that all the characteristic diffraction peaks of as-synthesized Cu₂O coincide well with those of cubic phase of Cu₂O and there are no peaks of impurities appeared in the XRD patterns. The peaks at 29.5, 36.4, 42.2, 61.3, 73.4, and 77.3° belong to the Bragg reflections of (1 1 0), (1 1 1), (2 0 0), (2 2 0), (3 1 1) and (2 2 2) plans of Cu₂O. The same situation is found in the case of CuO that the pure monoclinic phase of CuO is obtained in our study and the corresponding peaks at 32.8, 35.9, 39.0, 49.2, 61.8, and 68.1° belong to the Bragg reflections of (1 1 0), (1 1 1), (1 1 1), (2 0 2), (1 1 3) and (2 0 0).

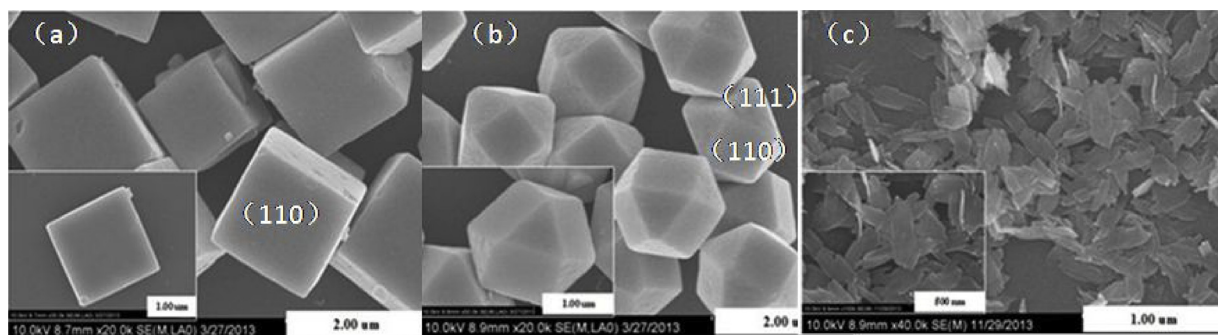


Fig. 1. SEM images of (a) Cu₂O(I), (b) Cu₂O(II), and (c) CuO.

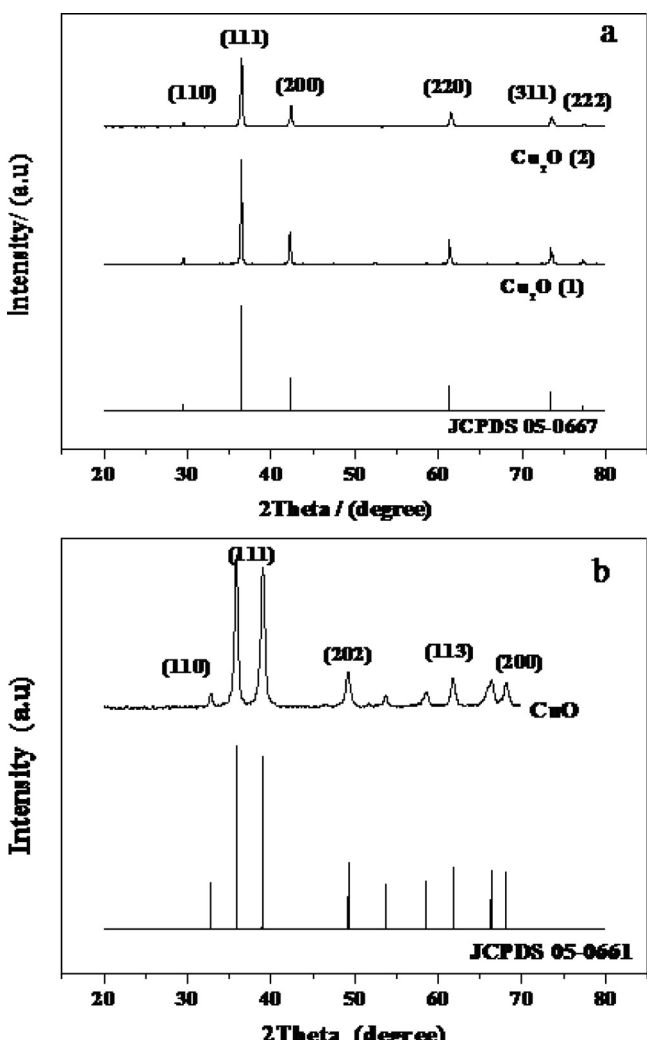


Fig. 2. XRD patterns of (a) as-synthesized cubic (1) and octahedral (2) Cu₂O and (b) sheet CuO.

plans of CuO. The above results indicate that the prepared oxides of copper are homogeneous in size together with good crystallinity and purity.

3.2. Deposition of gold nanoparticles on the as-synthesized CuOx

3.2.1. The structure of as-prepared Au-CuOx samples

A comparison was made in **Fig. 3** for the XRD patterns of Cu₂O with two morphologies and the corresponding Au/Cu₂O catalysts prepared by the modified deposition-precipitation method as well as sheet CuO

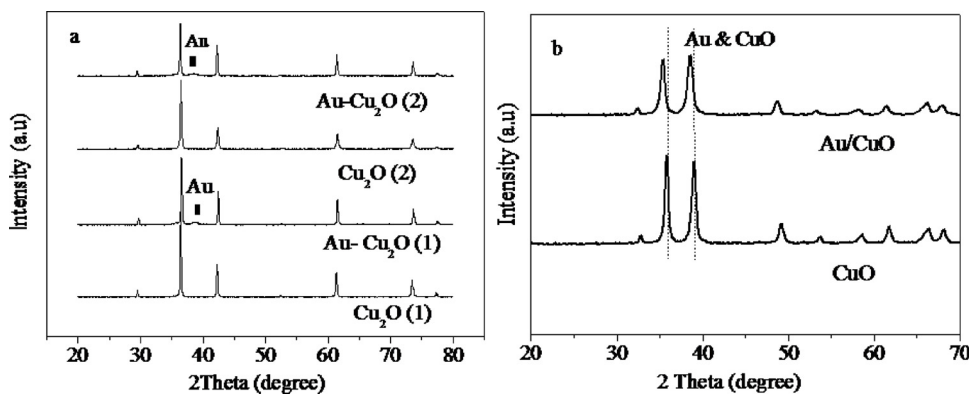


Fig. 3. XRD patterns of (a) Au/CuO with cubic (1) and octahedral Cu₂O (2) and (b) Au/CuO with sheet CuO.

and Au/CuO. In the left side of Fig. 3a, the XRD patterns of two Au-Cu₂O samples are as the same as the XRD patterns of Cu₂O except for a weak characteristic diffraction peak of Au at $2\theta = 38.5^\circ$ appeared (JCPDS card No. 4-784), no shift of the diffraction peaks of Cu₂O is found. This indicates that gold particles are loaded on two kinds of Cu₂O without modification of the structure and the crystal lattice parameters of Cu₂O. Gold particles are most probably absorbed on the surface of Cu₂O rather than in the lattice of Cu₂O [39,40].

As shown in Fig. 3b, no obvious diffraction peak of gold is found in the XRD patterns of Au/CuO when comparing with CuO sample. However, the characteristic diffraction peak of gold at $2\theta = 38.5^\circ$ is coincided with the diffraction peak of (1 1 1) of CuO at $2\theta = 38.6^\circ$. One can see that the positions of two CuO diffraction peaks in the sample of Au/CuO shift to a little lower degree than those in the sample of pure CuO and the peak at higher position become stronger due to introduction of gold. This highly suggests that the diffraction peak of gold at $2\theta = 38.5^\circ$ overlaps with that of CuO at $2\theta = 38.6^\circ$ and some gold nanoparticles are probably patched in the lattice of CuO.

3.2.2. The morphologies of as-prepared Au/CuOx samples and the dispersion of gold nanoparticles

A traditional preparation method in our lab, i.e., the modified deposition–precipitation method was employed to introduce gold particles into the as-prepared oxides of copper in the study. The SEM-EDX analysis was carried out to check any change in morphologies of CuOx and the truly introduction of gold in as-prepared Au/CuOx catalysts. The corresponding SEM images with elemental line-scan EDX results are displayed in Fig. 4 for the Au/Cu₂O samples.

Clearly, after the loading of gold, the smooth Cu₂O whatever cubic (in up side of Fig. 4) or cub-octahedron (in down side of Fig. 4) becomes rough, the cub-octahedron one more pronounced. However, the skeleton and size of Au/Cu₂O maintains well, which means that there are no damage of Cu₂O structure during loading gold. The results from line-scan EDX for two kinds of Cu₂O indicates the truly presence of gold in the prepared catalyst samples [41].

Different from the Au/Cu₂O samples, no clear change can be found from the SEM images of Au/CuO sample when comparing with that of sheet CuO (not shown). However, the elemental line-scan result surely identifies the introduction of gold into sheet of CuO. The presence of gold deposited into the prepared two cuprous oxides and the copper oxide was further confirmed by the inductively coupled plasma analysis which presented relatively higher gold loadings of 1.53, 1.46, and 1.82 wt% in Au/Cu₂O(cubic), Au/Cu₂O(octahedral), and Au/CuO(sheet), respectively.

High resolution transmission electron microscopy was employed to further observe the dispersions of gold particles on the as-synthesized CuOx materials. As shown in Fig. 5, the dispersion situation of gold particles on cubic Cu₂O and sheet CuO are quite different. Gold particles smaller than 10 nm are homogeneously dispersed on sheet CuO in

the shape of flat with a mean diameter of 4.0 ± 0.36 nm (see inset of Fig. 5b), indicating a strong contact between gold particles and the substrate of copper oxide. In contrast, due to the damage of smooth surface of Cu₂O crystals in the process of deposition of gold, some larger gold particles seem being located in the bushes grown from the Cu₂O body as indicated by red cycles. Most of gold particles should locate on or close to the surface of Cu₂O support; however, it is hard to get a clearer image because these delicate bushes are easily melted in TEM measurement.

F. Menegazzo et al. have demonstrated that CO chemisorption performed by a pulse flow system at -116°C can be taken as a method for the quantitative determination of the gold dispersion on mild reduced and hydrated Au/Fe₂O₃, Au/TiO₂ and Au/ZrO₂ catalysts [42,43]. In the present work we therefore alternatively performed pulse flow CO chemisorption measurements at the temperature of -116°C over the mild reduced samples of Au/CuOx together with the corresponding CuOx supports as references to the TEM observations. Since we do not have the device to do hydration treatment in our system which was adopted to avoid the CO chemisorptions on uncoordinated support ions, instead, the CO cumulative quantity on gold particles alone was calculated by subtracting CO uptake value on bare supports from that on the catalysts.

The samples of gold deposited on sheet CuO and cubic Cu₂O are chosen to perform pulse CO chemisorption measurements. The results of CO uptake value on the two samples are reported in left size of Table 2 together with gold loadings determined by AAS-ICP analysis. The dispersions and mean diameters of gold particles which were estimated by assuming a 1:1 chemisorption stoichiometry of adsorbed CO molecules on gold atoms were also included. It is evident that the CO chemisorbed volume per mole of gold is four times higher on the Au/sheet CuO sample than on the Au/cubic Cu₂O sample, indicating more homogeneous dispersion of gold particles on sheet CuO than on Cu₂O, as reflected by the estimated values of dispersions and mean diameters of gold particles. A significant decrease of chemisorbed CO on Au/Cu₂O implies that the total adsorbing sites are less abundant on the sample, in which HRTEM analysis has roughly revealed the presence of bigger gold particles which are unable to adsorb CO. In case of Au on sheet CuO, from Fig. 5b, we can see that most of gold particles are deposited on sheet CuO in a flattened shape, which is a normal deposition shape of gold particles when gold nanoparticles are supported on reducible oxides [42,44,45]. A relatively smaller value of 2.29 nm of mean diameter of gold particles estimated by pulse CO chemisorption was given compared with the TEM observation. It can be proposed that gold nanoclusters with size below 2 nm, which are not detectable by HRTEM, are present on Au/CuO, where almost all the atoms are exposed at the surface.

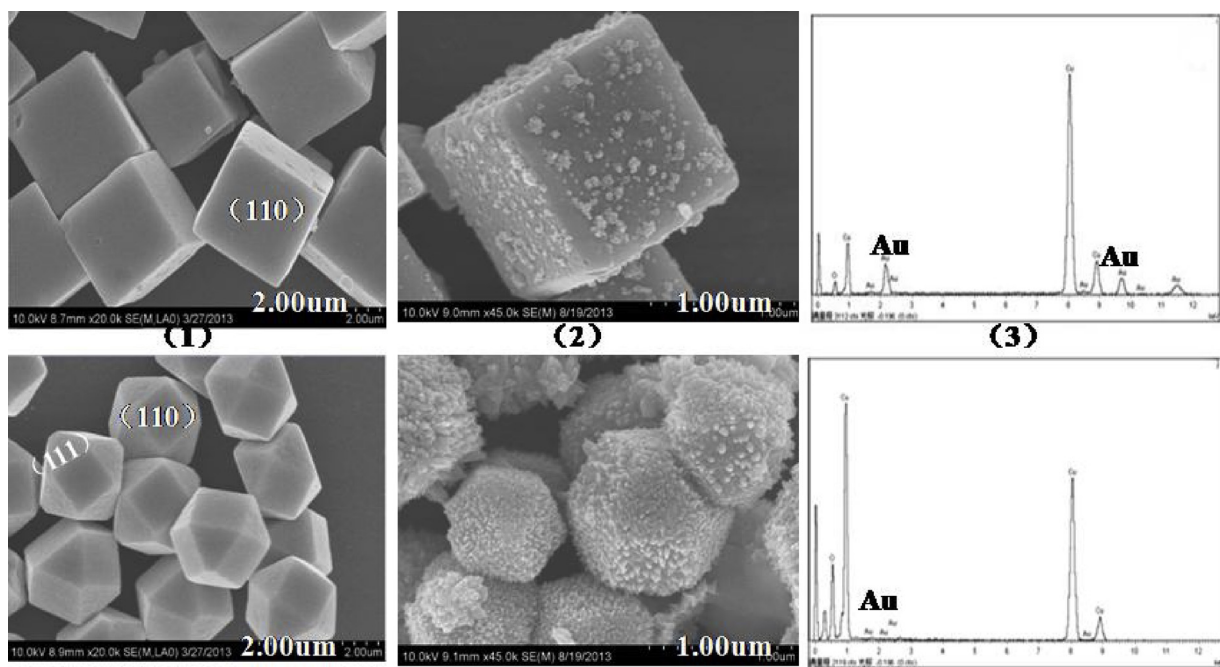


Fig. 4. SEM images of (1) Cu₂O, (2) Au/Cu₂O and (3) line-scan EDX patterns of Au/Cu₂O.

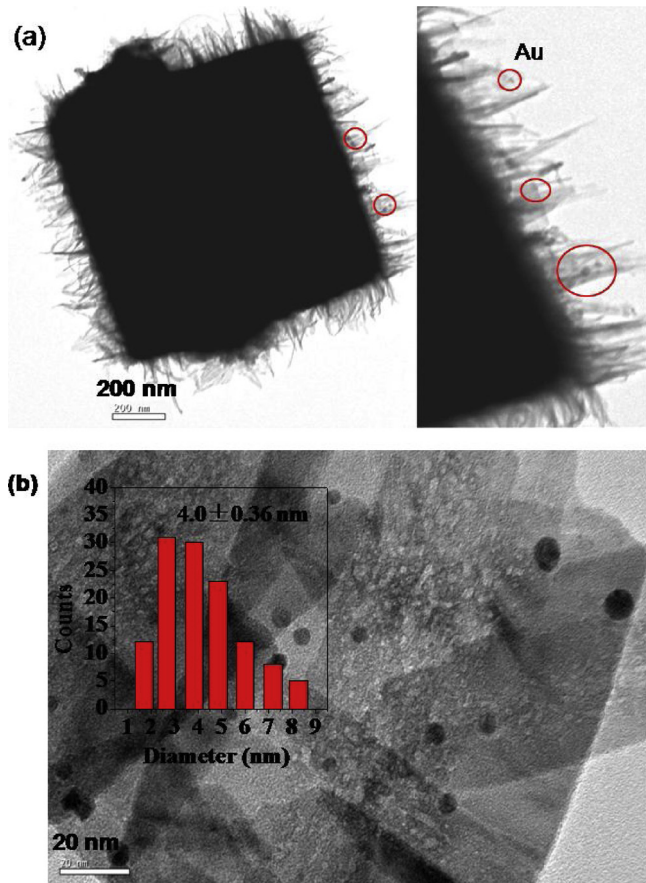


Fig. 5. TEM pictures of (a) Au/cubic Cu₂O and (b) Au/sheet CuO.

3.3. The chemical states of Au and Cu in the Au/CuOx catalysts

X-ray photoelectron spectroscopy was performed to clarify the chemical oxidation states of gold and copper in dried, unreduced samples of Au-CuOx catalysts. As shown in right side of Fig. 6, the

binding energies of Cu 2p 3/2 and Cu 2p 1/2 in the spectra of Cu 2p are nearly the same for the three fresh catalysts and which are located at 933.7 eV and 953.4 eV, respectively. To be mentioned that one obvious shakeup peak obviously popped up in the spectra of Cu 2p in the two Au-Cu₂O catalysts at around 940 eV, which can be attributed to Cu²⁺.

In contrast, there is no shakeup peak in the Cu 2p spectra of two Cu₂O samples before loading gold as shown in the Fig. 7. This suggests a simultaneous electron transfer between Au³⁺ to Cu⁺, leading to being oxidized of Cu₂O to CuO. The oxidized Cu₂O species means those on the surface and being contacted with gold particles. The observation of Au⁺ species in the XPS spectra of gold 4f in the samples of two Au/Cu₂O catalysts shown in left side of Fig. 6 also support this conclusion. On the other hand, it can be seen that for the dried sample of Au/CuO, Au³⁺ species is document. The existence of Au⁺ species is quite possibly a result of partially reduction of Au³⁺ in drying process. In simple, in the dried Au/Cu₂O sample, Au⁺-Cu²⁺ assemblies are dominant on the surface of Cu₂O substrate while both of Au³⁺-Cu²⁺ and Au⁺-Cu²⁺ entireties are existed in the dried Au/CuO sample.

3.4. The reducibility of Au and Cu in Au/CuOx catalysts

Since the reduction of oxidic copper and oxidic gold would occur in the CO-PROX reaction, the H₂-TPR analysis was performed to study the reducibility of the Cu₂O and CuO together with the corresponding gold catalysts. The Cubic Cu₂O and cub-octahedral Cu₂O samples show similar reductive performances. The representative H₂-TPR curve observed on the cubic Cu₂O sample is presented in Fig. 8. The reduction of Cu⁺ started at 177 °C and finished at 363 °C with the strongest reduction peak at 300 °C, as shown by line a in Fig. 8. This result is in good accordance with the research of others [34]. For the reduction of CuO, the reduction peak appears at 150 °C, which is lower for 27 °C compared with the starting reduction temperature of Cu₂O (see line c). The difference of finished temperature for the reduction of Cu₂O and CuO is small. The area of the reduction peak of CuO is much larger than Cu₂O with a wide reductive band, which is attributed to the overlap of the reductive band for Cu²⁺ to Cu⁺ and Cu⁺ to Cu⁰ [46,47].

The starting and finishing reduction temperatures and the area of the reduction peak of Au/Cu₂O in solid line b are almost same with those of Cu₂O in line a except for an additional shoulder peak at lower

Table 2Pulse CO chemisorption data at 116 °C and the formation of CO₂ over the Au/CuOx samples.

Samples	Au loading (wt%)	mL _{CO(STP)} /g _{cat}	mol _{CO} / mol _{Au}	Au dispersion (%)	Diameter of Au (nm)	React T °C	Con. %	Sel. %		Formation rate of CO ₂
								mol _{CO₂} 10 ⁻⁴ /g _{cat} h	mol _{CO} / mol _{Au} h	
Au/cubic Cu ₂ O	1.53	0.0605	0.034	5.0 [*]	-	23.3	50	2.75	100	0.122
						100	21.4	84.6	1.45	1.87
Au/sheet CuO	1.82	0.175	0.148	50.9 [*]	4.0 [#]	2.29 [*]	50	41.3	77.0	2.56
						100	95.3	60.0	4.58	4.96
Ratio				4.35 ^a						4.84 ^b /2.66 ^c

Ratio a: the ratio of molCO/molAu on Au/CuO to that on Au/cubic Cu₂O; ratio b: the ratio of CO₂ formation rate at 50 °C on Au/CuO to that on Au/cubic Cu₂O; ratio c: the ratio of CO₂ formation rate at 100 °C on Au/CuO to that on Au/cubic Cu₂O.

* The data was estimated by CO chemisorptions with 1:1 chemisorption stoichiometry of CO on Au atom.

Counted and calculated by HRTEM observation.

position of 230 °C. This weak peak at 230 °C in line b is quite possible related to the reduction of copper (II) oxide species [40] which is formed via an automatically inner electron transfer from part of Cu⁺ species to Au³⁺ in the Au/Cu₂O catalyst dried at 60 °C, as detected by above XPS analysis. The reduction of Au⁺ in line b is hardly recognized because of almost no change in the hydrogen adsorption amount corresponded to the later position of reduction peak and may be overlapped with the reduction peak of Cu⁺ in the sample.

On the other hand, the starting and finishing reduction temperatures of the reduction peak of Au/CuO in line d clearly shifts to lower position than those of CuO in line c, indicating that the deposition of nanogold particles increase the reducibility of sheet CuO. The obvious increase in the area of the overlapped reduction peak of Au³⁺, Cu²⁺, Au⁺ and Cu⁺ implies the occurrence of strong interactions between gold nanoparticles and CuO, leading to better reducibility in the contact areas [48].

3.5. The catalytic performance of Au catalysts

We firstly did the blank activity testing experiments over three oxides of copper both in oxygen-rich and hydrogen-rich atmospheres for the oxidation of CO. As shown in Fig. 9, the activity sequence of three samples is sheet CuO > cubic Cu₂O > cub-octahedron Cu₂O. The lowest temperatures for the complete conversion of CO over them in O₂-rich stream are 175, 198, and 218 °C, respectively. Both Cu(II) and Cu(I) species are active for the oxidation of CO, the former is a little

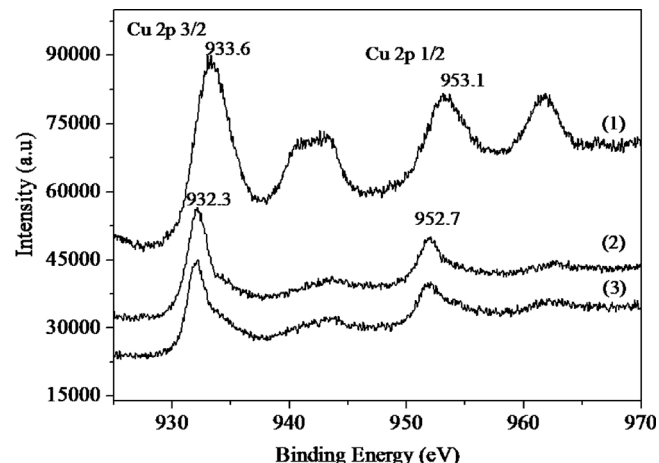


Fig. 7. XPS spectra of Cu 2p for (1) cubic Cu₂O, (2) octahedral Cu₂O, and sheet CuO.

more active than the latter. On the other hand, in the case of the CO-PROX reaction, the sheet CuO, cubic Cu₂O and cub-octahedron Cu₂O show the maximum conversions of CO at 150, 250 and 250 °C, respectively. The corresponding maximum conversions are 71%, 58.3%, and 34.2% with selectivities of 44%, 36%, and 22%, respectively. The CuO sample is certainly more active than Cu₂O although they have

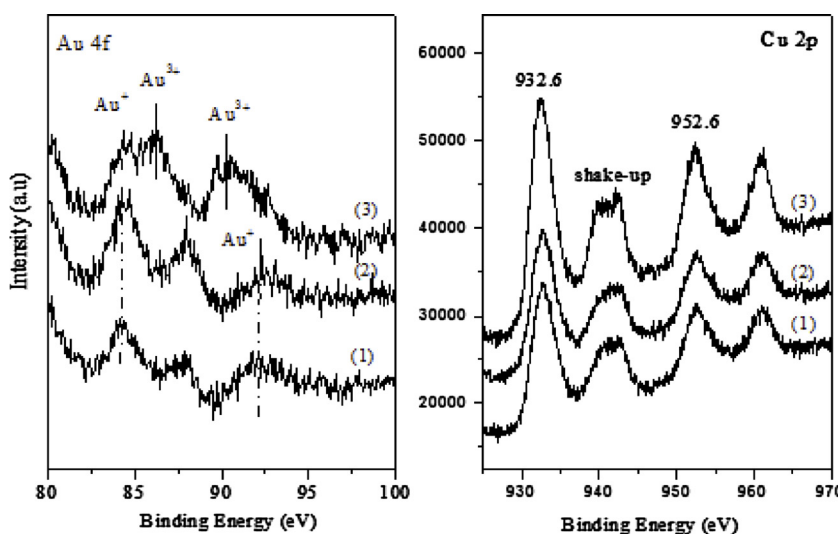


Fig. 6. XPS spectra of (a) Au4f and (b) Cu 2p for (1) Au/cubic Cu₂O, (2) Au/octahedral Cu₂O, and (3) Au/sheet CuO.

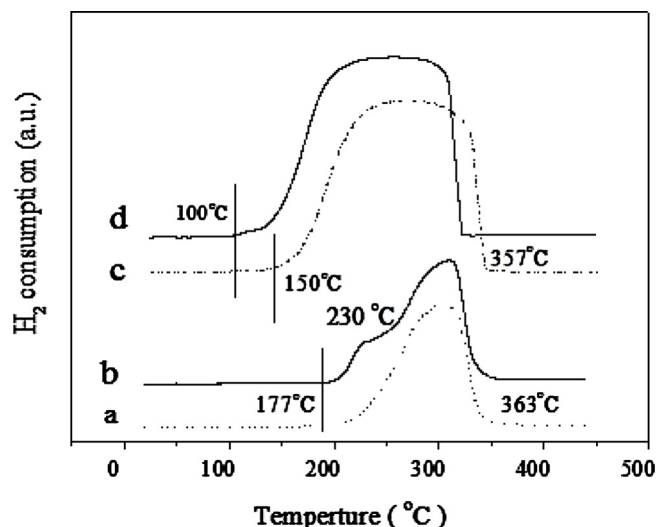


Fig. 8. H₂-TPR spectra of (a) Cu₂O (cubic), (b) Au/Cu₂O(cubic), (c) CuO(sheet), and (d) Au/CuO(sheet) samples.

similar light off temperature at around 50 °C. This meets the results on CO oxidation over the powdered CuO and Cu₂O sample which was done by Nagase et al. [49] and carbon monoxide oxidation over copper oxide supported on alumina done by Pierron et al. [50]. Pierron et al. also reported a phenomenon that the formation of lattice heterogeneities due to the reduction of cupric oxide resulted in the generation of reduced copper phases, leading to an improved activity than the reaction happened on pure Cu₂O phase. As shown in right size of Fig. 9, we observed same phenomenon over the two Cu₂O samples at reaction temperature higher than 200 °C, where the reduction of Cu₂O and formation of metallic Cu occurs.

After gold deposited on the three copper oxides, as shown in left side of Fig. 10, the complete conversion of CO over the Au/CuO catalyst can be achieved at 55 °C in oxygen-rich atmosphere, which is 120 °C lower than that of pure CuO in Fig. 9, indicating that the introduction of nanogold particles considerably enhances the catalytic activity of CuO, showing the cooperation effects between Au and CuO for the CO oxidation as mentioned in the literatures [10–13,16]. However, slight enhancement is observed over the two Cu₂O samples after the deposition of gold only when the reaction temperatures are below 150 °C.

In H₂-rich atmosphere, a maximum CO conversion of 95.3% with a selectivity of 60% at 100 °C is observed over Au/CuO catalyst. The specific value for CO₂ formation rate at 100 °C is calculated as 4.97 mol_{CO₂}/mol_{Au} h, comparable to most active and selective CO-PROX catalysts studied in the published works [10–13,16–19,51–53]. Higher CO conversion and CO₂ selectivity at lower reaction temperature was obtained when comparing with the CO-PROX results over CuO itself in Fig. 9, again demonstrating the cooperation effects between Au and CuO for the CO oxidation.

On the other hand, similar enhancement in catalytic performance over the two Au/Cu₂O catalysts is, however surprisingly observed this time. Much higher CO conversions of 83 and 70% and CO₂ selectivity of 52 and 45% are obtained at lower reaction temperature of 150 °C than those values on the two Cu₂O samples in Fig. 9. The corresponding catalytic performance for the CO-PROX reaction over six samples with and without gold deposition is presented in Table 3. It is easier to conclude that Au addition largely decreases the complete conversion temperature of CO with clearly enhancement in selectivity to CO₂, i.e., gold considerably improved the catalytic performance of copper oxides for the CO-PROX reaction. In addition, in above all cases, the catalytic activities of Au-Cu₂O (Cubic) is little higher than those of Au-Cu₂O (cub-Octahedron).

4. Discussion

The oxidation state of copper may changes thermodynamically between CuO, Cu₂O and Cu as a function of temperature depending on oxygen-rich or hydrogen-rich atmospheres. From Fig. 9, we can see that the conversions of CO over CuO varying with reaction temperatures are almost same at temperatures below 150 °C in both reactive streams, regardless of oxygen-rich or hydrogen-rich. The temperature for the maximum conversion of CO over CuO in hydrogen-rich atmosphere is at around 150 °C which just meet the starting reduction temperature of CuO (see Fig. 8, line c), indicating the loss of catalytic activity due to the formation of cupric oxide. Thinking together with the considerable decrease in CO conversion over Cu₂O in H₂-rich reaction stream, we may conclude that the active sites for CO oxidation either in oxygen-rich or hydrogen-rich streams should be associated with the phases of copper oxide. The close activity of Cu₂O to CuO in oxygen-rich atmosphere (left side in Fig. 9) could be a result of partial oxidation of Cu₂O to CuO.

Our H₂-TPR and XPS characterizations demonstrate that in the dried Au/Cu₂O sample, Au⁺–Cu²⁺ assemblies are dominant on the surface of

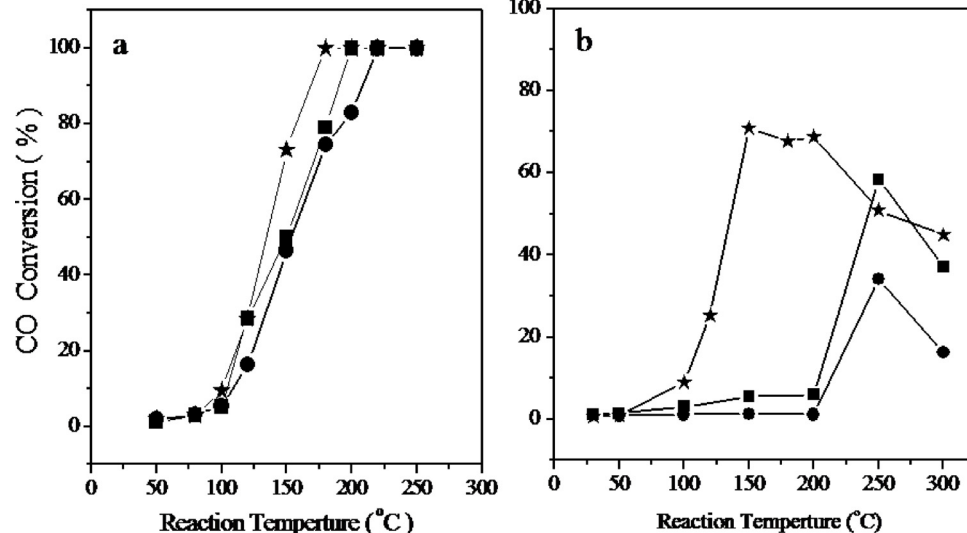


Fig. 9. CO oxidation over CuO (★), cubic Cu₂O (■), and octahedral Cu₂O (●) in (a) oxygen-rich stream (1.0 vol.% CO, 21 vol.% O₂, 78 vol.% N₂, 50 ml/min, 0.2 g Cat.) and (b) hydrogen-rich stream (1.2 vol.% CO, 0.8 vol.% O₂, 50 vol.% H₂, 48 vol.% N₂, 50 ml/min, 0.2 g Cat.).

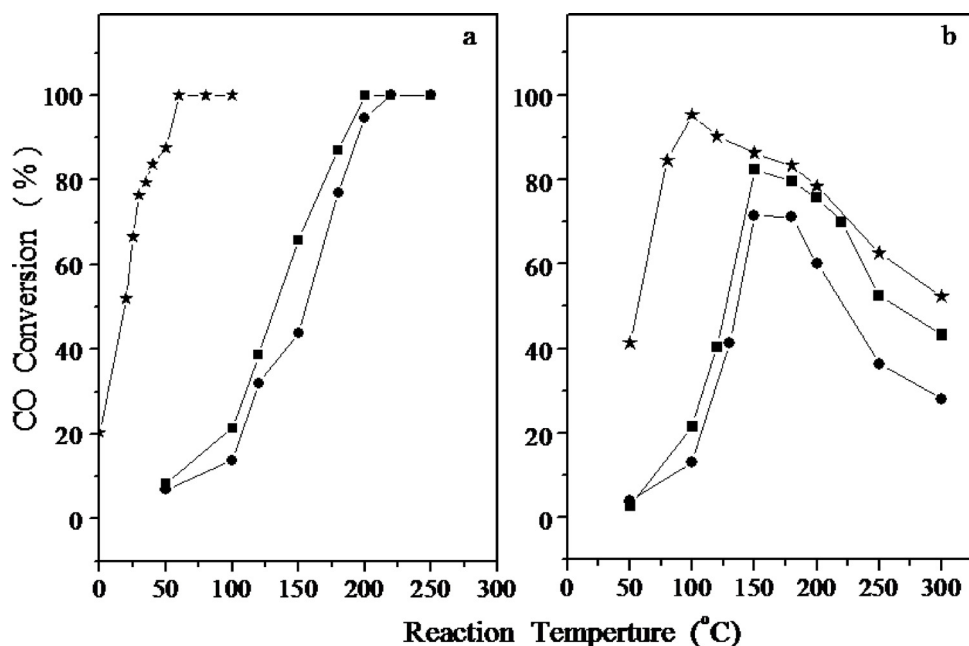


Fig. 10. CO oxidation over Au/sheet-CuO (○), Au/cubic Cu₂O (□), and Au/octahedron Cu₂O (△) in (a) oxygen-rich stream (1.0 vol.% CO, 21 vol.% O₂, 78 vol.% N₂, 50 ml/min, 0.2 g Cat.) and (b) hydrogen-rich stream (1.2 vol.% CO, 0.8 vol.% O₂, 50 vol.% H₂, 48 vol.% N₂, 50 ml/min, 0.2 g Cat.).

Table 3
The CO-PROX reaction over oxides of copper with and without nanogold.

Catalysts	Max. CO Conv.	Sel. @ max. CO Conv. (%)	Formation rate of CO ₂ (molCO ₂ 10 ⁻⁴ /g _{cat} h)
	T (%)	Con. (%)	
Cubic			
Cu ₂ O	250	58	36
Au-Cu ₂ O	150	83	3.47
Octahedral			
Cu ₂ O	250	35	22
Au-Cu ₂ O	150	70	45
Sheet			
CuO	150	70	45
Au-CuO	100	95	4.58

Cu₂O substrate while Au³⁺-Cu²⁺ are dominantly existed in the dried Au/CuO sample. In process of CO oxidation, the oxygen-rich atmosphere will not change the chemical states of gold and copper in fresh catalysts, the reaction results may reflect the catalytic capability of these cationic Au and Cu species. However, hydrogen-rich streams in CO-PROX reaction, a strong reducing atmosphere, will quite possibly reduce these cationic species during reaction with an increase in reaction temperature and thus tune dynamically the catalytic performance.

It is worth to note that Cu(II) species are existed in all of three as-prepared oxides of copper supported Au catalysts. The fair comparison in the catalytic performance after gold deposition should be made mainly with the performance of CuO in O₂-rich and H₂-rich reactive streams.

A comparison of the catalytic curves of Au/CuO in Fig. 10 with those of CuO in Fig. 9, no matter in O₂-rich or H₂-rich reactive stream, clearly shows the significant enhancement in catalytic activity of the CO oxidation, reflecting the cooperation effect between nanogold and CuO substrate. The lower activity over Au/CuO in H₂-rich than in O₂-rich stream implies a suppression of hydrogen in CO oxidation over gold catalysts via a complete reaction of hydrogen oxidation, which is in agreement with our previous study [16].

Comparing the catalytic curves of two samples of Au/Cu₂O in Fig. 10 with the curves of CuO in Fig. 9, we can see similar curves of two samples to those of CuO both in oxygen-rich stream and especially

in hydrogen-rich stream (right side of two figures). Interestingly, slight enhancement in the CO conversions over the samples with gold, especially the sample of Au/cubic Cu₂O, was found only when the reaction temperatures below 150 °C, regardless of O₂-rich or H₂-rich atmospheres. This demonstrates the cooperation effect between gold and CuO species at certain extent and the Cu(II)O species in two samples of Au/Cu₂O play a main role in the reaction of CO oxidation.

XPS analysis were done on three as-prepared gold catalyst samples after CO-prox reaction at different reaction temperatures in order to correlate the chemical states of gold and copper with the corresponding catalytic performance of CO oxidation due to possible reduction in H₂-rich stream. As shown in Fig. 11, the shake-up peak, the characteristic peak of Cu(II)O can be observed at temperatures below a value of the maximum conversion of CO, i.e., 100 °C for the Au/CuO catalyst (left side of Fig. 11) and 150 °C for the Au/Cu₂O sample (right side of Fig. 11). The shake-up peak of Cu(II)O disappears and other two peaks corresponded to CuO at 932.3 and 952.2 eV become narrower and slightly shift to lower energy position when the reaction temperatures are higher than the value of the maximum conversion of CO, indicating a decrease in activity occurs when reduction of Cu(II)O starts in H₂-rich reactive stream. The XPS analysis results for the spent catalysts further confirm our above deduction on the importance of CuO species and the cooperation effects between CuO and nanogold particles for the oxidation of CO. However, why is the Au/sheet CuO much more active than other two samples of Au/Cu₂O?

Our SEM and TEM characterizations and pulse CO chemadsorption measurements in Section 3.2.2 explored that over CuO and Cu₂O, the contact situation of gold particles are quite different. In case of Au/CuO, the smaller gold nanoparticles were flatly attached with CuO substrate, demonstrating a strong contact between them, whereas in the case of Au/Cu₂O, larger Au particles seem to be loosely contacted with CuO bush which is resulted from automatically oxidation of Cu₂O by Au³⁺ in preparation process. Due to introduction of gold into CuO substrate, the significant increase in reducibility of CuO measured by H₂-TPR analysis in Fig. 8 and the disturbing of crystal lattices of CuO detected by XRD in Fig. 3b also imply the strong interaction occurred between gold nanoparticles and CuO substrate.

In the present work, as-synthesized CuO and Cu₂O substrates are non-porous, the dispersion situation of nanogold particles on their

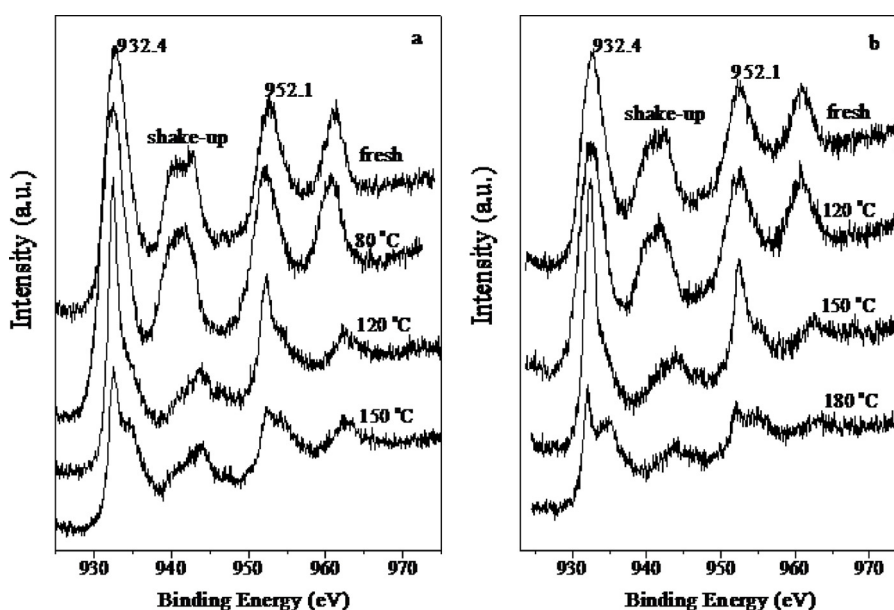


Fig. 11. XPS patterns of spent catalysts of (a) Au/CuO and (b) Au/Cubic Cu₂O at different reaction temperatures.

surface is a key matter for their catalytic performance. The CO chemisorbed volume per mole of gold over the catalyst of Au/sheet CuO in Table 2 is four times more than that on the Au/cubic Cu₂O sample, indicating much higher dispersion of Au nanoparticles on sheet CuO than on Cu₂O. The reaction rates in terms of CO₂ formation rate at temperatures of 50 and 100 °C are evaluated and compared between the two catalysts at same reaction temperature. As shown in right side of Table 2, the CO₂ formation rate over Au/sheet CuO is 3 to 5 times of that over Au/cubic Cu₂O. It should mention that the sample with higher CO/Au molar ratio is more active in the CO-PROX reaction, thus suggesting a strong correlation between catalytic activity and gold particles dispersion, even if other factors are certainly relevant to catalytic activity.

In short, our work in this study confirms the importance of CuO species and the cooperation effect between CuO and nanogold particles for the CO-PROX reaction. Strong correlation between catalytic activity and the dispersion of gold particles was found too. The cooperation effect between CuO and nanogold can considerably improved the activity of the Au/CuO catalyst only when the strong contact between them occurred, demonstrating the importance of the Au/metal oxide interface for CO oxidation reaction addressed in several articles [32,54]. It is worthy to emphasize that the chemical states of Au seem less important than interface interaction between gold and oxide substrate for the CO oxidation. The debate concerning cationic Au or metallic Au as the active sites for the oxidation of CO and other reactions [32,54,55] is still no final conclusion. The observation from this study may shed light on a depth understanding for gold catalysis.

5. Conclusions

We controllably synthesized two kinds of Cu₂O with different morphologies and sheet CuO. Deposition of nanogold particles was carried out by using the modified deposition-precipitation method. Two kinds of reactive environment, i.e., the oxidation of CO in hydrogen-rich stream and the reaction of CO oxidation in oxygen-rich stream were adopted to evaluate three as-prepared CuO/Cu₂O substrates and the corresponding supported gold catalysts without further reduction. XRD, SEM, BET, H₂-TPR, XPS techniques were performed to characterize the structure, composition, and chemical states of key elements of the catalysts. The main conclusions have been drawn as following:

- (1) XRD and SEM results show that nanogold particles do not enter the Cu₂O crystal lattice, but attached to the surface of the cuprous oxide, well maintaining specific morphology and crystal structure of Cu₂O. While nanogold particles smaller than 10 nm flatly deposit on CuO surface, leading to strong interaction between them with maintaining the morphology of sheet CuO.
- (2) During the preparation process, the oxidation-reduction reaction automatically occurred between Au³⁺ and Cu⁺ for two as-prepared samples of Au/Cu₂O. Our H₂-TPR and XPS characterizations reveal that in two dried, as-prepared Au/Cu₂O sample, Au⁺-Cu²⁺ assembles are mainly existed on the surface of Cu₂O substrate while both of Au³⁺-Cu²⁺ and Au⁺-Cu²⁺ entirties are deposited in the dried Au/CuO sample but the former is dominant.
- (3) The activity sequence for CO oxidation in both of O₂-rich and H₂-rich reactive stream is Au-CuO > Au-Cu₂O and cubic Au-Cu₂O > cub-octahedron Au-Cu₂O. The morphologies of the oxides of copper have much less influence than chemical states of copper in the catalytic performance of the CO oxidation.
- (4) The CuO not Cu₂O species play a more critical role for the oxidation of CO. The cooperation effect between CuO and nanogold can considerably enhance the activity of the Au/CuO catalyst only when the strong interaction between them occurred.

Acknowledgements

This work was financially supported by the Key Research and Development Plan of Shandong Province (no. 2018CXGC1108) and the Natural Science Foundation of China (nos. 21603181 and 21773202). Caixia Qi gratefully acknowledges the financial support of the Shandong Taishan Scholarship, Yantai double-hundreds talents plan and “152 talents program” from Yantai University. We also acknowledged the financial supports from the Collaborative Innovation Center of Light Hydrocarbon Transformation and Utilization.

References

- [1] K. Liu, A.Q. Wang, T. Zhang, ACS Catal. 2 (6) (2012) 1165.
- [2] L.S. Xu, Y.S. Ma, Y.L. Zhang, Z.Q. Jiang, W.X. Huang, J. Am. Chem. Soc. 131 (45) (2009) 16366.
- [3] T. Niu, G.L. Liu, Y. Liu, Appl. Catal. B Environ. 154–155 (2014) 82.
- [4] C. Wang, L. Zhang, Y. Liu, Appl. Catal. B Environ. 136–137 (2013) 48.
- [5] M. Haruta, N. Yamada, T. Kobayashi, S. Iijima, J. Catal. 115 (1989) 301.
- [6] M. Daté, M. Haruta, J. Catal. 201 (2001) 221.

- [7] I. López, T. Valdés-Solís, G. Marbán, Int. J. Hydrogen Energy 33 (2008) 197.
- [8] Z. Wu, H. Zhu, Z. Qin, H. Wang, L. Huang, J. Wang, Appl. Catal. B Environ. 98 (2010) 204.
- [9] C.G. Maciel, L.P.R. Profeti, E.M. Assaf, J.M. Assar, J. Power Sources 196 (2011) 747.
- [10] J. Fonseca, H.S. Ferreira, N. Bion, Lirault-Roy, M.C. Ranhel, D. Duprez, F. Epron, Catal. Today 180 (1) (2012) 34.
- [11] P. Sangeetha, B. Zhao, Y. Chen, Ind. Eng. Chem. Res. 49 (2010) 2096.
- [12] T.S. Mozer, D.A. Dziuba, C.T.P. Vieira, F.B. Passos, J. Power Sources 187 (2009) 209.
- [13] A. Alihoseinzadeh, A.A. Khodadadi, Y. Mortazavi, Int. J. Hydrogen Energy 39 (2014) 2056.
- [14] J.L. Santos, T.R. Reina, S. Ivanova, J.A. Odriozola, Applied. Catal. B Environ. 201 (2017) 310.
- [15] Q. Jia, D. Zhao, B. Tang, N. Zhao, H. Li, Y. Sang, N. Bao, X. Zhang, X. Xu, H. Liu, J. Mater. Chem. A 2 (38) (2014) 16292.
- [16] X. Sun, H. Su, Q. Lin, C. Han, Y. Zheng, L. Sun, C. Qi, Appl. Catal. A Gen. 527 (2016) 19.
- [17] J.C. Bauter, D. Mullins, M. Li, Z. Wu, E.A. Payzant, S.H. Overbury, S. Dai, Phys. Chem. Chem. Phys. 13 (2011) 2571.
- [18] A. Sandoval, C. Louis, R. Zanella, Appl. Catal. B Environ. 140–141 (2013) 363.
- [19] X. Li, S.S. Fang, J. Teo, Y.L. Foo, A. Borgna, M. Lin, Z.Y. Zhong, ACS Catal. 2 (2012) 360.
- [20] G.J. Hutchings, M.S. Hall, A.F. Carley, P. Landon, B.E. Solsona, C.J. Kiely, A. Herzing, M. Makkee, J.A. Moulijn, A. Overweg, J.C. Fierro-Gonzalez, J. Guzman, B.C. Gates, J. Catal. 242 (2006) 71.
- [21] M.F. Camellone, S. Fabris, J. Am. Chem. Soc. 131 (2009) 10473.
- [22] B. Qiao, J.-X. Liang, A. Wang, C.Q. Xu, J. Li, T. Zhang, J. Liu, Nano Res. 8 (2015) 2913.
- [23] D. Stolicic, M. Fischer, G. Ganterförl, Y.D. Kim, Q. Sun, P. Jena, J. Am. Chem. Soc. 125 (2003) 2848.
- [24] L.D. Socaciu, J. Hagen, T.M. Bernhardt, L. Wöste, U. Heiz, H. Hakkinen, U. Landman, J. Am. Chem. Soc. 125 (2003) 10437.
- [25] H. Tang, Y. Su, B. Zhang, A.F. Lee, M.A. Isaacs, K. Wilson, L. Li, Y. Ren, J. Huang, M. Haruta, B. Qiao, X. Liu, C. Jin, D. Su, J. Wang, T. Zhang, Sci. Adv. 3 (2017) 10606.
- [26] L.W. Guo, P.P. Du, X.P. Fu, C. Ma, J. Zeng, R. Si, Y.Y. Huang, C.J. Jia, Y.W. Zhang, C.H. Yan, Nat. Commun. 7 (2016) 13481.
- [27] T.J. Huang, D.H. Tsai, Catal. Lett. 87 (2003) 173.
- [28] A. Hornes, A.B. Hungría, P. Bera, A.L. Camara, M. Fernandez-García, A. Martínez-Arias, L. Barrio, M. Estrella, G. Zhou, J. Fonseca, J.J.C. Hanson, J.A. Rodriguez, J. Am. Chem. Soc. 132 (2010) 34.
- [29] D. Gamarra, M. Fernandez-García, C. Belver, A. Martínez-Arias, J. Phys. Chem. C 114 (2010) 18576.
- [30] D. Gamarra, C. Belver, M. Fernandez-García, A. Martínez-Arias, J. Am. Chem. Soc. 129 (2007) 12064.
- [31] F.C. Duh, D.S. Lee, Y.W. Chen, Modern Res. Catal. 2 (2013) 1.
- [32] M. Haruta, Faraday Discuss. 152 (2011) 11.
- [33] H. Bao, W. Zhang, D. Shang, Q. Hua, Y. Ma, Z. Jiang, J. Yang, W. Huang, J. Phys. Chem. C 114 (14) (2010) 6676.
- [34] Y. Sui, W. Fu, H. Yang, Y. Zeng, Y. Zhang, Q. Zhao, Y. Li, X. Zhou, Y. Leng, M. Li, G. Zou, Cryst. Growth Des. 10 (1) (2009) 99.
- [35] C.H. Kuo, M.H. Huang, J. Am. Chem. Soc. 130 (38) (2008) 12815.
- [36] L. An, S. Qi, X. Zou, WO Patent 007774 A1 (2006).
- [37] C. Qi, H. Su, R. Guan, X. Xu, J. Phys. Chem. C 116 (2012) 17492.
- [38] C. Qi, S. Zhu, H. Su, H. Lin, R. Guan, Appl. Catal. B Environ. 138–139 (2013) 104.
- [39] C.H. Kuo, T.E. Hua, M.H. Huang, J. Am. Chem. Soc. 131 (49) (2009) 17871.
- [40] Q. Hua, F. Shi, K. Chen, S. Chang, Y. Ma, Z. Jiang, G. Pan, W. Huang, Nano Res. 4 (10) (2011) 948.
- [41] Z. Wang, S. Zhao, S. Zhu, S. Zhu, Y. Sun, M. Fang, CrystEngComm 13 (7) (2011) 2262.
- [42] F. Menegazzo, M. Manzoli, A. Chiorino, F. Bocuzzi, T. Tabakova, M. Signoretto, F. Pinna, N. Pernicone, J. Catal. 237 (2006) 431.
- [43] F. Menegazzo, F. Pinna, M. Signoretto, V. Trevisan, F. Bocuzzi, A. Chiorino, M. Manzoli, Appl. Catal. A Gen. 356 (2009) 31.
- [44] M. Valden, X. Lai, D.W. Goodman, Science 281 (1998) 1647.
- [45] C.T. Campbell, Science 306 (2004) 234.
- [46] M. He, M. Luo, P. Fang, J. Rare Earths 24 (2) (2006) 188.
- [47] J.L. Ayastuy, E. Fernández-Puertas, M.P. González-Marcos, Int. J. Hydrogen Energy 37 (9) (2012) 7385.
- [48] R.J. Chimentao, F. Medina, J.L.G. Fierro, J. Llorca, J. Sueiras, Y. Cesteros, P. Salagre, J. Mol. Catal. A: Chem. 274 (2007) 159.
- [49] K. Nagase, Y. Zheng, Y. Kodama, J. Kakuta, J. Catal. 187 (1999) 123.
- [50] E.D. Pierron, J.A. Rashkin, J.F. Roth, J. Catal. 9 (1967) 38.
- [51] T.R. Reina, S. Ivanova, O.H. Laguna, M.A. Centeno, J.A. Odriozola, Appl. Catal. B Environ. 197 (2016) 62.
- [52] Q. Lin, B. Qiao, Y. Huang, L. Li, J. Lin, X. Liu, A. Wang, W. Li, T. Zhang, Chem. Commun. 50 (2014) 2721.
- [53] X. Liao, W. Chu, X. Dai, V. Pitchon, Appl. Catal. B Environ. 142–143 (2013) 25.
- [54] R.A. Ojifinni, N.S. Froemming, J. Gong, M. Pan, T.S. Kim, J.M. White, G. Henkelman, C.B. Mullins, J. Am. Chem. Soc. 130 (2008) 6801.
- [55] M.P. Casaleotto, A. Longo, A. Martorana, A. Prestianni, A.M. Venezia, Surf. Interface Anal. 38 (2006) 215.